Nonlinear Dynamics and Systems Theory, **20** (1) (2020) 21–37

Control Design for Non-Linear Uncertain Systems via Coefficient Diagram Method: Application to Solar Thermal Cylindrical Parabolic Trough Concentrators

Z. Fenchouche [1*], M. Chakir [1], O. Benzineb [2], M.S. Boucherit [1] and M. Tadjine [1]

[1] *Automatic Control Department, LCP, National Polytechnic School, Algeria*
[2] *Electronics Department, University of Blida, Blida, Algeria*

Received: June 21, 2019; Revised: December 30, 2019

Abstract: In this paper, we propose a new application of the coefficient diagram method (CDM) to design a robust controller of non-linear uncertain system, the control is applied to a distributed collector field of a solar power plant based on cylindrical parabolic trough concentrators. The non-linear uncertain system is represented by two PDEs of both the fluid and the metal. To design the control, a linearization of the non-linear system is made around an equilibrium point to have a transfer function, this point represents the simulation's steady state of the real system, then the controller is obtained using the form of Manabe for the CDM. Comparing the results of this method with those of the PID controller, it is shown that the CDM design is an easy and robust control for a non-linear system, that gives enhanced stability with good settling time with respect to the large rise time.

Keywords: *coefficient diagram method (CDM); partial differential equation (PDE); cylindrical parabolic trough concentrator; nonlinear uncertain system.*

Mathematics Subject Classification (2010): 93C10, 93D09.

* Corresponding author: mailto:zakaria.fenchouche@g.enp.edu.dz

1 Introduction

In the last decade, renewable energies have received more and more attention in order to meet the exponential growth of energy demand. Among renewable energies, the interest in solar energy has increased, many solar electricity systems were developed, such as concentrated solar thermal, and more precisely, cylindrical-parabolic trough collectors (Fig. 1), which are the most used technologies for concentrating solar energy. Today, some plants are under construction, while others are already operating, such as the Platform Solar of Almeria (ACUREX) [1].

The main problem in solar energy sources is the independency of the solar radiation variations, in addition, it can not be adjusted to suit demands that we desire. We note, for example, cloud cover, humidity and air transparency as atmospheric conditions that may affect the solar radiation by unpredictable variations [2].

From the perspective of research, many works have been proposed to either model, control or observe the system [1]. The authors in [3–7] have given different models of the solar system with different levels of complexity and accuracy, like the bilinear reduced or the non-linear distributed system [1].

On the other side, many automatic control strategies have been implemented, that is to make the plant work close to the nominal operating point. In what follows, we cite well known tests experimented at the plant ACUREX: with a self-tuning PID controller in [2], in [8] the authors have designed a fuzzy logic controller, the model predictive control (RMPCT) has been implemented in [9], etc. Additionally, other controller's strategies are based on the predictors and the estimators of variables like effective solar radiation or the system's temperature as in [10].

It is well known that even with a development in the control side, the PID remains a very important controller in the industry with a percentage of 95 % among the controllers used in the practice [11]. However, many constraints are imposed in the practical applications as noted in the previous reference, such as the upper limit of magnitude of the control signal, the unexpected non-linear effects occurred by the saturation or others. For these reasons, it is necessary to develop a robust control application to obtain better control performances of double integrating unstable systems, where the stability is not ensured by the PID controller which is developed for stable systems [12].

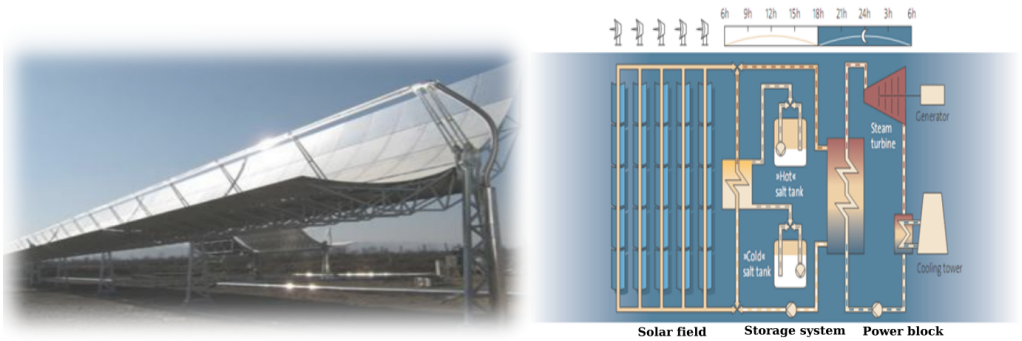

Figure 1: Parabolic distributed solar collector with the schematic diagram of solar thermal hydraulic circuit.

Hence, in this work we propose the use of an algebraic approach that has proved its

robustness in several works. It is a new robust controller known as a Coefficient Diagram Method (CDM), developed for uncertain systems and introduced by many researchers such as Manabe, see [13], [14] and [15] (it is important to note that we will not talk about the advanced controls applied in other works, because we are interested in controls to apply in practical and in industrial systems such as PID and RQG).

The CDM is based on a spatial diagram called a coefficient diagram, which is used as a vehicle to carry the necessary design information and as a criteria of good design. The method is recently used because of the simplest and robust controller that can be found for any plant under practical limitations, in addition, this simplicity makes it very powerful for systems with various uncertainties. In other words, the CDM can give a controller design which is both stable and robust, and has the desired system response speed, and also is less sensitive to disturbances and parameter variations, without overshoots and is obtained for specified settling time [16].

This paper is organized as follows. First, the solar plant is described in Section 2 with the system modelling, approximations, discretization and linearization. Subsequently, the CDM structure and its design are presented in Section 3 followed by its application on the plant in Section 4. Then, numerical tests and simulations to assess the robustness and stability of the controller are also shown in this section. Finally, Section 5 summarizes the obtained results.

2 Solar Power Plant Description and Modeling

2.1 Plant description

Most of the thermo-plants in the world use the cylindrical-parabolic collectors because of their significant energy productivity, and the simplicity of the method. It consists of linear parabolic mirrors that reflect and concentrate solar energy (irradiations) on a metal tube which represents the receiver that is positioned along a focal line. This allows to heat oil, used as a heat-transfer fluid (HTF), to reach temperatures that ensure evaporation on the level of the turbine (Fig. 1).

Moreover, the Platform ACUREX of ALMERIA is a well-known station in the field of research. It consists of 10 loops, each one is made up of two lines of 12 modules, and the length of each loop is 172 m, it also consists of a pump with a limited operation between the maximum capacity 12 L/s and the safety threshold 2 L/s.

2.2 Plant modeling

The distributed solar collector field can be described by a distributed parameter model of the temperature while considering general assumptions and hypotheses. The model is represented by the following system of partial differential equations (PDE) which describes the energy balance [17]:

$$\frac{\partial T_f}{\partial t} = \frac{\delta_p H_t}{\rho_f C_f A_f}(T_m - T_f) - \frac{q}{A_f}\frac{\partial T_f}{\partial l}, \tag{1}$$

$$\frac{\partial T_m}{\partial t} = \frac{K_{opt}\eta_0 G}{\rho_m C_m A_m} I - \frac{G H_l}{\rho_m C_m A_m}(T_m - T_a) - \frac{\delta_p H_t}{\rho_m C_m A_m}(T_m - T_f), \tag{2}$$

where the subindex m refers to the metal and that of f to the fluid. The parameters of the system and their values are given in Table 1, where

$$H_v = 2.17 \times 10^6 - 5.01 \times 10^4 T_f + 4.53 \times 10 T_f^2 - 1.64 T_f^3 + 2.1 \times 10^{-3} T_f^4, \tag{3}$$

T_{in}, T_{out} and T_a are the inlet temperature, the outlet temperature and the ambient temperature, respectively.

Parameter	Description	Value	Unit
δ_p	Wet perimeter	0.1257	m
ρ_f	Density of f	903 - 0.672.T$_f$	kg.m^{-3}
C_f	S.H.C of f	1820 + 3.478.T$_f$	J.kg$^{-1}{}^{\circ}C^{-1}$
D_f & D_m	Diameters	0.04 & 0.07	m
A_f & A_m	Sections	0.0013 & 0.0038	m^2
H_t	C.H.T.C	q$^{0.8}H_v$	W.$^{\circ}C^{-1}$m^{-2}
H_l	C.H.T.C	0.00249 $\Delta\bar{T}$ - 0.06133	W.$^{\circ}C^{-1}$m^{-2}
I	Irradiation	variable	W.m^{-2}
q	Fluid flow	to control	m^3.s^{-1}
K_{opt}	Optical efficiency	$\eta_{opt} = \eta_0.K_{opt} = 0.7$	—
η_0	Collector efficiency		—
G	Collector aperture	$= \delta_p.\pi = 1.83$	—
ρ_m	density of m	1100	Kg.m^{-3}
C_m	S.H.C of m	840	J.Kg^{-1}.$^{\circ}C^{-1}$
$\Delta\bar{T}$	—	$= \left(\frac{T_{in}+T_{out}}{2} - T_a\right)$	$^{\circ}C$

Table 1: Parameters description.

Many authors used different simplified models, based on simplified energy balances, such as neglecting heat losses, or controlling the system using just one equation which corresponds to the variation of the fluid temperatures. However, the system should be used under a non-simplified model, as described in equations (1) and (2), to have an accurate control. Hence, that is the first contribution of this paper.

The aim of our work is to control the outlet temperature of the tube denoted $T_{out}(t) = T_f(t, L)$ around a set-point. The incoming energy depends on several parameters such as the efficiency of the collectors, the mirror reflectivity and on the effective reflecting surface.

We used this model for control synthesis and simulation. The parameters and the properties of the fluid used may be considered constant or variable depending on the variations of the temperature. We also remind that the flow of the fluid is comprised between

$$2\,L.s^{-1} \leq q \leq 12\,L.s^{-1}, \tag{4}$$

and the difference between T_{out} and T_{in} must be less than 80 °C:

$$T_{out} - T_{in} \leq 80\ ^{\circ}C. \tag{5}$$

The first equation of the PDEs obtained from the energy balance, contains two differentials depending on space (x) and time (t). For simplification reasons, the first differential will be eliminated using a discretization on the space as mentioned in Fig. 2, so we discretize the system on $\frac{n}{2}$ segments ($\frac{n}{2}$ is just a token, to have a dimension of the system equal n which will be explained in Section 2.3, and it represents the number of segments of the tube). In this case, we may introduce a truncation error

$$\frac{\partial T_f}{\partial l} = \frac{T_f(l_i) - T_f(l_{i-1})}{\Delta l} + \Theta(\Delta l). \tag{6}$$

But, as long as this approximation of the derivative may not be very accurate for the control synthesis, the truncation error will be added to the general perturbation terms.

Hence, we rewrite the first system as follows :

$$\frac{\partial T_f(l_i)}{\partial t} = \frac{\delta_p H_t}{\rho_f C_f A_f}(T_m(l_i) - T_f(l_i)) - \frac{q}{A_f.\Delta l}(T_f(l_i) - T_f(l_{i-1})), \tag{7}$$

$$\frac{\partial T_m(l_i)}{\partial t} = \frac{K_{opt}\eta_0 G}{\rho_m C_m A_m} I - \frac{GH_l}{\rho_m C_m A_m}(T_m(l_i) - T_a) - \frac{\delta_p H_t}{\rho_m C_m A_m}(T_m(l_i) - T_f(l_i)), \tag{8}$$

where the state vector is as follows:

$$X = [T_f(l_1)\, T_f(l_2)\, \cdots T_f(l_{\frac{n}{2}})\, T_m(l_1)\, T_m(l_2) T_m(l_3) \cdots T_m(l_{\frac{n}{2}})]^T$$

$$= [x_1\, x_2\, \cdots x_{\frac{n}{2}-1}\, x_{\frac{n}{2}}\, x_{\frac{n}{2}+1}\, x_{\frac{n}{2}+2}\, \cdots x_{n-1}\, x_n]^T, \tag{9}$$

and

$$\begin{cases} x_1 &= T_{out}, \\ x_{\frac{n}{2}} &= T_{in}. \end{cases} \tag{10}$$

Also, we write the system equations in the following state form:

$$\begin{cases} \dot{X} &= F(X,u), \\ Y &= h(X) \qquad = x_1, \end{cases} \tag{11}$$

where

$$u \;=\; q(t), \tag{12}$$

and

$$dim(\dot{X}) \;=\; dim(X) \;=\; n \times 1. \tag{13}$$

$\dot{X}$ is given by

$$\dot{X} = F(X,u) = \begin{bmatrix} \frac{\delta_p.H_t(1)}{\rho_f(1).C_f(1).A_f}(x_{\frac{n}{2}+1} - x_1) - \frac{u}{A_f.\Delta_l}(x_1 - x_2) \\ \frac{\delta_p.H_t(2)}{\rho_f(2).C_f(2).A_f}(x_{\frac{n}{2}+2} - x_2) - \frac{u}{A_f.\Delta_l}(x_2 - x_3) \\ \vdots \\ \frac{\delta_p.H_t(\frac{n}{2}-1)}{\rho_f(\frac{n}{2}-1).C_f(\frac{n}{2}-1).A_f}(x_{n-1} - x_{\frac{n}{2}-1}) - \frac{u}{A_f.\Delta_l}(x_{\frac{n}{2}-1} - x_{\frac{n}{2}}) \\ \frac{\delta_p.H_t(\frac{n}{2})}{\rho_f(\frac{n}{2}).C_f(\frac{n}{2}).A_f}(x_n - x_{\frac{n}{2}}) - \frac{u}{A_f.\Delta_l}(x_{\frac{n}{2}} - T_{in}) \\ \frac{K_{opt}\eta_0 G}{\rho_m C_m A_m} I - \frac{GH_l}{\rho_m C_m A_m}(x_{\frac{n}{2}+1} - T_a) - \frac{\delta_p H_t(1)}{\rho_m C_m A_m}(x_{\frac{n}{2}+1} - x_1) \\ \frac{K_{opt}\eta_0 G}{\rho_m C_m A_m} I - \frac{GH_l}{\rho_m C_m A_m}(x_{\frac{n}{2}+2} - T_a) - \frac{\delta_p H_t(2)}{\rho_m C_m A_m}(x_{\frac{n}{2}+2} - x_2) \\ \vdots \\ \vdots \\ \frac{K_{opt}\eta_0 G}{\rho_m C_m A_m} I - \frac{GH_l}{\rho_m C_m A_m}(x_n - T_a) - \frac{\delta_p H_t(n)}{\rho_m C_m A_m}(x_n - x_{\frac{n}{2}}) \end{bmatrix}$$

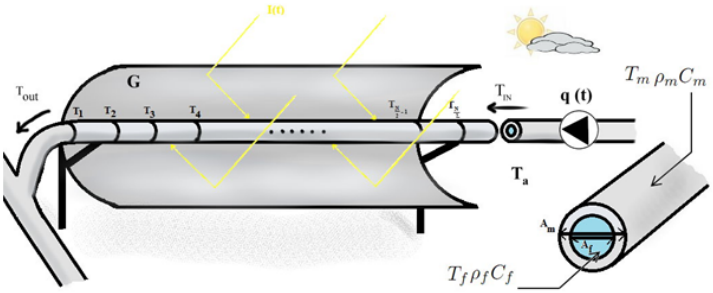

Figure 2: Diagram of the collector showing parameters and spatial discretization.

2.3 Operating point and control model

In this work we use the three blocks structure of Fig. 3 based on the CDM. This method requires the transfer function of the system, but knowing that the model is non-linear, we must have a linearization around an operating point $P_0(x_0, u_0)$.

Besides, to have $\dot{X} = 0$, this point must be an equilibrium point where the state is steady, we propose to use the results of real simulations of controls applied on the ACUREX in some works such as [18]. For the linearization we will use Taylor's series.

Using Taylor's series we get the system

$$\begin{cases} \dot{X} \simeq \dot{X}_0 + \frac{\partial F}{\partial X} \mid_{(X_0,u_0)} (X - X_0) + \frac{\partial F}{\partial u} \mid_{(X_0,u_0)} (u - u_0) + \zeta(X, u), \\ Y \simeq \frac{\partial h}{\partial X} \mid_{(X_0,u_0)}, \end{cases} \tag{14}$$

where

$$\begin{cases} u - u_0 &= \Delta u, \\ X - X_0 &= \Delta X, \\ Y - Y_0 &= \Delta Y, \end{cases} \tag{15}$$

and

$$(\dot{X - X_0}) = \dot{X} - \dot{X}_0 = \dot{X} \quad (\dot{X}_0 = 0). \tag{16}$$

Thus

$$\dot{\Delta X} = \dot{X}. \tag{17}$$

We take

$$\begin{cases} A_F &= \frac{\partial F}{\partial X} \mid_{(X_0,u_0)}, \\ B &= \frac{\partial F}{\partial u} \mid_{(X_0,u_0)}, \\ C &= \frac{\partial h}{\partial X} \mid_{(X_0,u_0)}. \end{cases} \tag{18}$$

Finally, the system may be written on state space eliminating the error of second order as follows :

$$\begin{cases} \dot{\Delta X} &= A_F.\Delta X + B.\Delta u, \\ \Delta Y &= C.\Delta X. \end{cases} \tag{19}$$

After the deduction of system matrices in state space, we conclude the transfer function $G(s)$:

$$G(s) = \frac{\Delta Y(s)}{\Delta U(s)} = C.(sI - A_F)^{-1}.B. \tag{20}$$

For the simulation, the number of the discretization segments is taken as desired, for example, 15. If so doing, the denominator of the transfer function calculated has, in general, $dim = n = 30$.

3 Recall on CDM Control Design

The CDM is a novel robust controller which uses an algebraic approach and is developed for uncertain non-linear systems. It is based on a spatial digram called a coefficient diagram [14, 19].

The design of the CDM controller is composed of three blocks (Fig. 3), $A(s)$ is the forward denominator polynomial, $F(s)$ and $B(s)$ are two numerators polynomials, the first for the reference and the second for feedback. These polynomials in this structure are designed to have better performance on tracking the desired reference signal and rejection disturbances, in addition to that, it helps to avoid the cancellation of unstable pole-zero. [14]

For the controller synthesis, we must have a transfer function, let it be $G(s)$, formed by the numerator $N(s)$ and the denominator $D(s)$.

The characteristic polynomial of the closed loop P(s) is as follows [20] :

$$P(s) = D(s)A(s) + N(s)B(s) = \sum_{i=0}^{n} a_i s^i. \tag{21}$$

To make the design of the CDM, we must also know three parameters on which the design is based, the equivalent time constant (τ), the stability indices (γ_i) and the stability limits (γ_i^*), they are defined in function of the coefficients of the characteristic polynomial [20, 21]:

$$\gamma_i = \frac{a_i^2}{a_{i+1}a_{i-1}}, \quad i = 1, ..., n-1, \tag{22}$$

$$\gamma_0 = \gamma_n = \infty, \tag{23}$$

$$\tau = \frac{a_1}{a_0}, \tag{24}$$

$$\gamma_i^* = \frac{1}{\gamma_{i-1}} + \frac{1}{\gamma_{i+1}}. \tag{25}$$

Using these relations between the parameters and the coefficients, the characteristic polynomial $P(s)$ (also called the target characteristic polynomial) can be formulated in terms of (τ) and (γ_i) as follows [15]:

$$P(s) = a_0 \left[\left\{ \sum_{i=2}^{n} \left(\prod_{j=1}^{i-1} \frac{1}{\gamma_{i-j}^i} \right) (\tau s)^i \right\} + \tau s + 1 \right]. \tag{26}$$

Note that we can give the expression of the equivalent time function of the settling time t_s as follows [15]:

$$\tau = \alpha . t_s, \qquad \alpha \in [0.33, \ \ 0.4]. \tag{27}$$

Many authors recommend the standard Manabe form to be used for the CDM design [14]. This form has been found after many studies, and stability indices have been chosen as [22]

$$\gamma_i = \{2.5, 2, 2, ..., 2\} \ \ for \ \ i = 1 \sim (n-1). \tag{28}$$

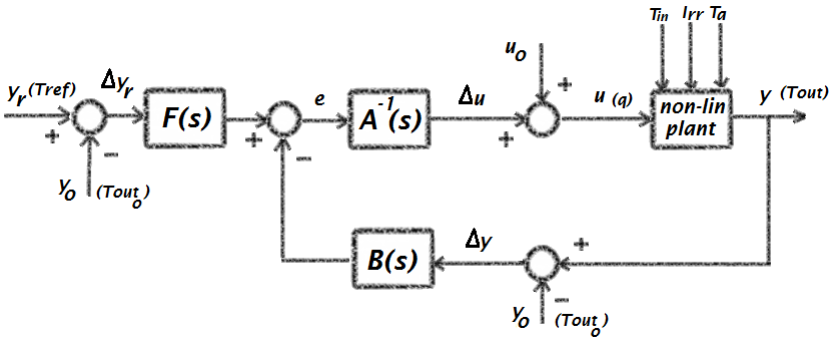

Figure 3: The block diagram of the CDM applied on the non-linear plant.

The procedure to design a controller using the CDM is given in [13]. Following this procedure step by step, we apply the method on our system.

Thus, the transfer function in polynomial form is given by

$$\frac{N(s)}{D(s)} = \frac{b_m s^m + b_{m-1} s^{m-1} + \cdots + b_1 s + b_0}{d_n s^n + d_{n-1} s^{n-1} + \cdots + d_1 s + d_0}, \tag{29}$$

where $N(s)$ and $D(s)$ are the numerator polynomial of degree m and the denominator polynomial of degree n, respectively, with $m \leq n$.

The controller structure shown in Fig. 3 is based on two polynomials, namely, A(s) and B(s), that are given by

$$A(s) = \sum_{i=0}^{p} l_i s^i, \qquad B(s) = \sum_{i=0}^{q} k_i s^i. \tag{30}$$

Many criteria are considered to choose the degree of the controller polynomials, where the perturbations are one of these criteria.

To define the degrees for the different cases of the disturbances, a table is given by [14], where n is given as a degree of the denominator's polynomial of the transfer function G(s), and the pre-controller defined by the polynomial $F(s)$ is chosen to be

$$F(s) = \left(\frac{P(s)}{N(s)} \right)_{|s=0}. \tag{31}$$

The coefficients of the controller polynomials are computed using the Diophantine equation given by

$$A(s)D(s) + B(s)N(s) = P(s). \tag{32}$$

We note that $P(s)$ is determined by substituting values of the parameters γ_i, a_0 and τ in the equation (26). γ_i, $_{i=\sim(n-1)}$ are chosen from the Manabe form. a_0 and τ are replaced by different values until we obtain the desired results.

D(s) and N(s) are given from the polynomial form of the transfer function of the system. It remains to find l_i and k_i being the parameters of $A(s)$ and $B(s)$, respectively, using the linear relation of coefficients [19].

For instance, with $m = 2, n = 3$ and taking the model of step disturbances, we have deg(P(s)) = 6, deg(B(s)) = 3 and deg(A(s)) = 3 with $l_0 = 0$. We can write

$$\begin{pmatrix} d_3 & 0 & 0 & 0 & 0 & 0 & 0 \\ d_2 & d_3 & 0 & b_2 & 0 & 0 & 0 \\ d_1 & d_2 & d_3 & b_1 & b_2 & 0 & 0 \\ d_0 & d_1 & d_2 & b_0 & b_1 & b_2 & 0 \\ 0 & d_0 & d_1 & 0 & b_0 & b_1 & b_2 \\ 0 & 0 & d_0 & 0 & 0 & b_0 & b_1 \\ 0 & 0 & 0 & 0 & 0 & 0 & b_0 \end{pmatrix} \begin{pmatrix} l_3 \\ l_2 \\ l_1 \\ k_3 \\ k_2 \\ k_1 \\ k_0 \end{pmatrix} = \begin{pmatrix} a_6 \\ a_5 \\ a_4 \\ a_3 \\ a_2 \\ a_1 \\ a_0 \end{pmatrix}, \tag{33}$$

which is also called the Sylvester form that can be shortened as follows:

$$[C]_{7\times 7} \begin{bmatrix} l_i \\ k_i \end{bmatrix}_{7\times 1} = [a_i]_{7\times 1}. \tag{34}$$

Parameters are simply calculated by solving the linear equation, then $F(s)$ can be computed by the equation (31):

$$\begin{bmatrix} l_i \\ k_i \end{bmatrix} = [C]^{-1}[a_i]. \tag{35}$$

Generally, after using the standard Manabe form, no adjustments in the parameters are needed, except when dealing with systems that require accurate control. In this case, we may need some adjustments after doing the first design of the controller, modifying the design parameters and repeating the process until getting the best response and desired results.

For instance, if the system reaches saturation, we may increase τ sufficiently and repeat the process. While decreasing τ can accelerate the response as desired.

4 Solar Plant Controller with CDM

The block diagram of CDM applied on the solar plant is shown on Fig. 3.

First, we choose an equilibrium point, and we linearize the system around this point. Taking P_0(T_{out} = 250 °C, T_{in} = 180 °C, I = 750 W/m^2, u = 7.3 L/s (0.0073 m^3.s^{-1})), the linear system around P_0 is represented by the following transfer function :

$$G(s) = \frac{-54.03s^{29} - 157.9s^{28} - ... - 1.945 \times 10^{-31}s}{s^{30} + 2.764s^{29} + ... + 3.868 \times 10^{-36}s} \frac{-3.27 \times 10^{-34}}{+3.846 \times 10^{-39}}, \tag{36}$$

where $G(s)$ is obtained from the formula in (20).

Model reduction: As we see, the denominator of $G(s)$ has $dim = n = 30$. Hence, the synthesis of the regulator is difficult because of the high order of the transfer function. In this case, we must reduce the order of our system, using a Matlab function that calculates the Gramians, it reduces the order from $dim = n$ to 2 or 3 as desired (*modred* function with *balreal*) to obtain a reduced function denoted G_r(s).

The transfer function $G_r(s)$ will be used only in synthesizing the regulator. Then, this regulator will be applied on the non-linear system.

Using the model reduction function we obtain

$$G_r(s) = \frac{N(s)}{D(s)} = \frac{-3610s^2 - 41.55s - 1.287}{s^2 + 0.00667s + 1.513 \times 10^{-5}}. \tag{37}$$

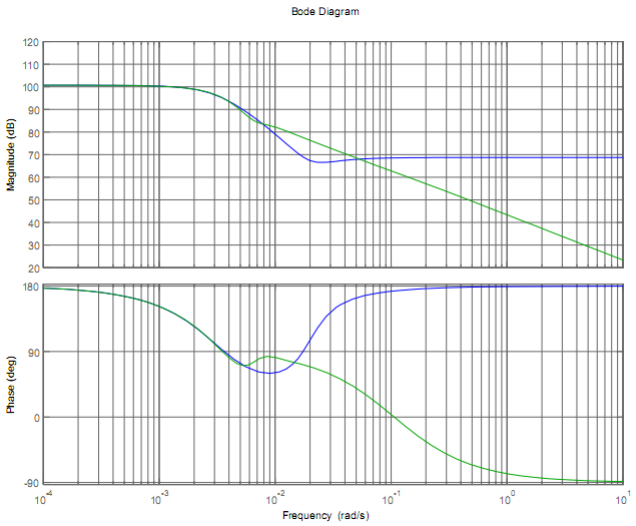

Figure 4: Comparison of the Bode diagram of G(s) model (in green) versus its approximated second-order model G_r(s) (in blue).

The comparison of the Bode diagram of G(s) model versus its approximated second-order model G_r(s) is given in Fig. 4.

It is seen that the reduced system magnitude and phase are the same as those of the original system in frequency less than $10^{-2}Hz$, for our case it does not impose a problem, because the study will be made in low frequencies.

Simulation will be done using Matlab and Simulink programs, where in Simulink we control the non-linear system with CDM and PID controllers in the structure shown before, this system is represented by two partial differential equations written in file of Matlab (file.m) and introduced to Simulink by s-function.

In this simulation, we will consider models related to step disturbances taking the $A(s)$ and $B(s)$ degrees according to the rules mentioned in the table given in [14] to get the correct polynomials.

For the CDM controller synthesis, we give values of τ and a_0 to find the polynomials using the Sylvester form. As mentioned in the method description in Section 3, we vary the value of τ until obtaining the best response.

In this case, we have

$$\tau = 278.5\ [s], \qquad a_0 = 0.4. \tag{38}$$

Thus, the controller polynomials are found as follows:

$$A(s) = 5836s^2 + 201900s, \tag{39}$$

$$B(s) = -5331s^2 - 74.17s - 0.3109, \tag{40}$$

and the pre-controller is given by

$$F(s) = \left(\frac{P(s)}{N(s)}\right)_{|(s=0)} = \frac{0.4}{-1.287} = -0.3109. \tag{41}$$

Controller	Response time	IAE	ISE	ITAE	Rise time	Settling time	Peak overshoot	Disturbance's peak
CDM	278.5 s	2472	15640	$2.525.10^7$	432 s	612 s	0 (0 %)	0 (0 %)
PID	270 s	5828	8156	$5.441.10^7$	108 s	1260 s	0.5 (5 %)	2.5 (25 %)

Table 2: Performance of CDM and PID controllers applied on the solar plant A.

Parameters of PID controller have been chosen using the block of PID controller in Simulink containing the PID tuning tool, knowing that a transfer function of a conventional PID controller is written as

$$G_c(s) = K_p(1 + \frac{K_i}{s} + sK_d), \tag{42}$$

where K_p is the proportional gain, K_I is the integral constant and K_D is the derivative constant.

We took PID parameters that ensure the best system's response according to stability, robustness and response time. These parameters correspond to the PID controller, where

$$K_p = -8.274.10^{-3}, \quad K_I = -6.412.10^{-4}, \quad K_D = 8.913.10^{-3} \tag{43}$$

(small values because the output of the controller is Δu with the unit $m^3.s^{-1}$).

4.1 Performances tests

The comparison between the two controllers is based on the following performance criteria. These criteria are based on the integral error, they are used as a good measure for evaluating the precision of the set point tracking and disturbances rejection [23].

IAE is the integral of the absolute tracking error which penalizes small errors [24]:

$$IAE = \int_0^\infty |e(t)|dt. \tag{44}$$

ITAE is the integral of the time-weighted absolute error which penalizes the errors that persist for a long time:

$$ITAE = \int_0^\infty te(t)dt, \tag{45}$$

and ISE is the integral of the tracking error squared which penalizes large errors:

$$ISE = \int_0^\infty e^2(t)dt. \tag{46}$$

For simulation, we propose a profile of variant inlet temperature, ambient temperature and solar irradiance that are shown in Fig. 5, Fig. 6 and Fig. 7, respectively (the profiles have been taken approximately to real values as used in other papers).

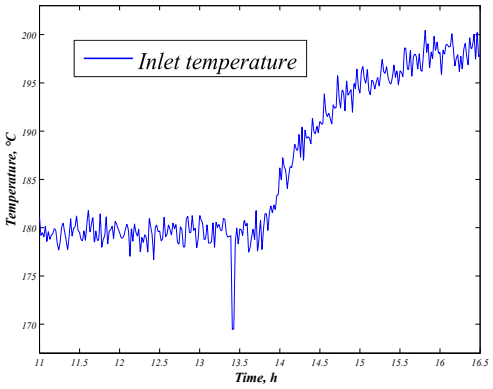

Figure 5: Inlet temperature.

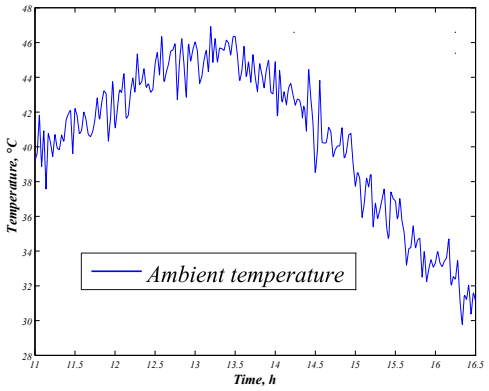

Figure 6: Ambient temperature.

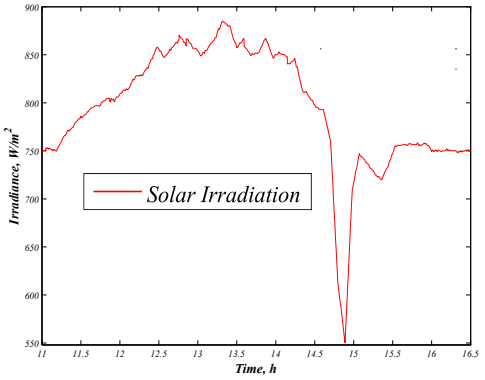

Figure 7: Solar irradiations.

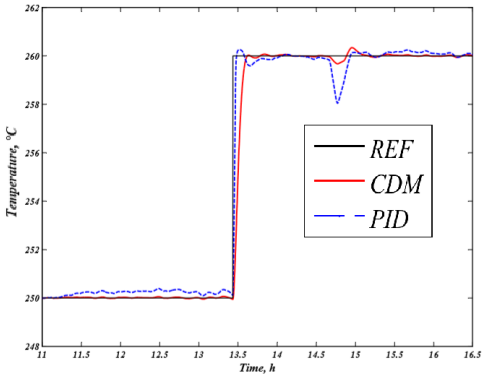

Figure 8: Response to a step reference for CDM and PID controllers.

Fig. 8 and Fig. 9 illustrate responses of CDM and PID controllers for a step reference with the corresponding fluid flow.

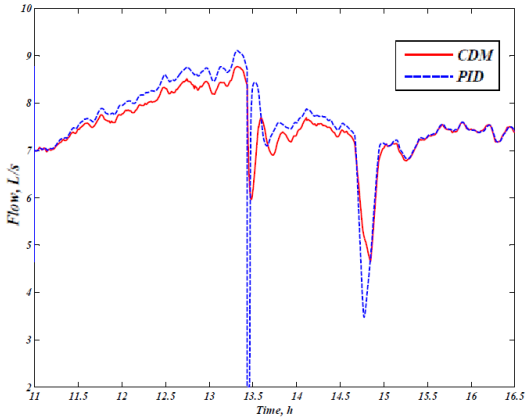

Figure 9: Fluid flow.

As we see in Table 2, the PID controller has better rise time. Nevertheless, the CDM

controller presents better performance indexes in comparison with the PID controller, with a better settling time with no peak overshoots or disturbance's peak. Except that, ISE is little wide because of the large rise time in the case of CDM controller response.

To make more tests to the CDM controller, we did another simulation for the 5 hours and half (between 11:00 and 16:30). The controllers were evaluated with reference variations (between $235°C$ and $265\ °C$), using the same profiles of variant solar irradiation, inlet temperature and ambient temperature.

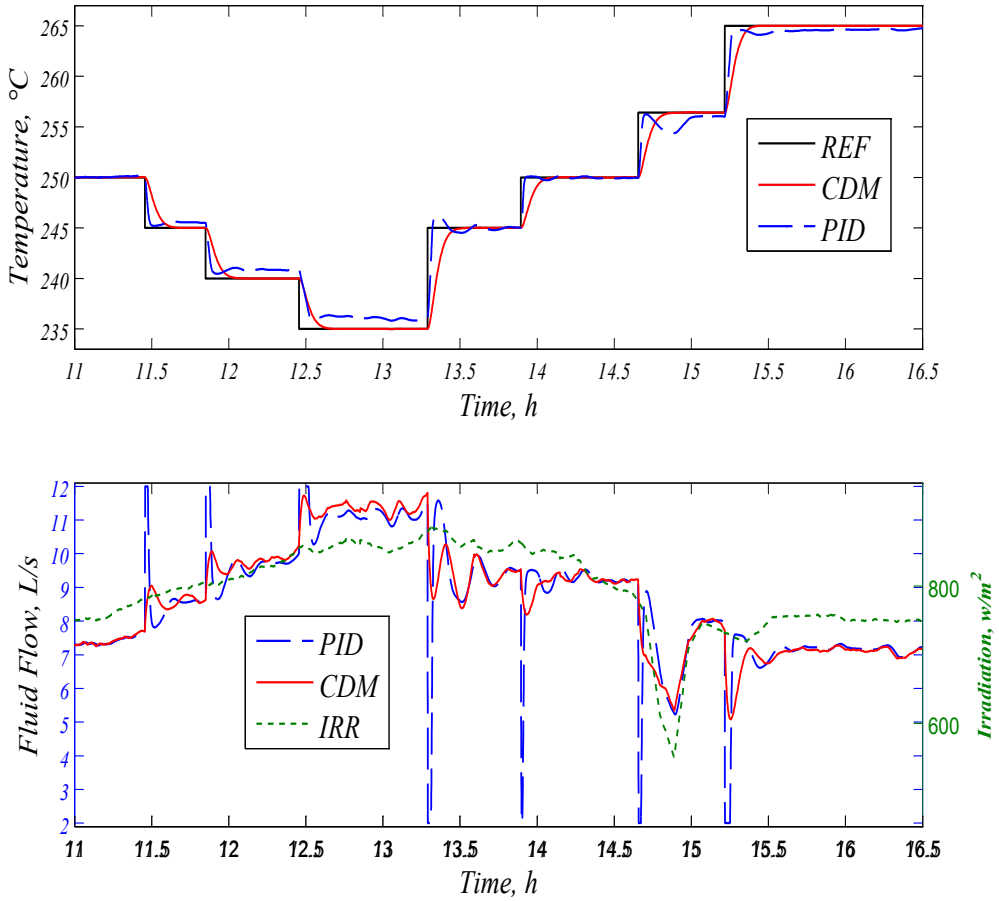

Figure 10: Reference temperature and average outlet temperature for the CDM (impulse-sinusoidal type disturbances) and PID controller.

From Fig. 10 and Table 3, it appears that the CDM exhibits better performance than the PID control, even with a large rise time compared to the first type, especially in the case of the supposed brutal change in the solar irradiance as an effect of the passing clouds (at 14,8 h) or the brutal change in the inlet temperature (at 13,5 h).

We also note that the pump's performance is better and widely admissible with instantaneous small impulses, which may give a considerable lifetime to this pump. Which is not the case in the PID controller with a huge impulses in case of reference variation.

Fig. 11 and Fig. 12 describe the temperature evolution inside the pipe in 2D and

Controller	IAE	ISE	ITAE
CDM	1.087×10^4	4.937×10^4	9.838×10^7
PID	1.375×10^4	2.747×10^4	1.299×10^8

Table 3: Performance of CDM and PID controllers applied on the solar plant B.

3D, respectively. The performance of CDM controller in terms of time response (settling time, even with a small rise time in comparison with the PID), reference tracking and disturbances rejection clearly appears in Fig. 11 where the outlet temperature tracks the reference even with disturbed inlet temperature with an admissible pump control.

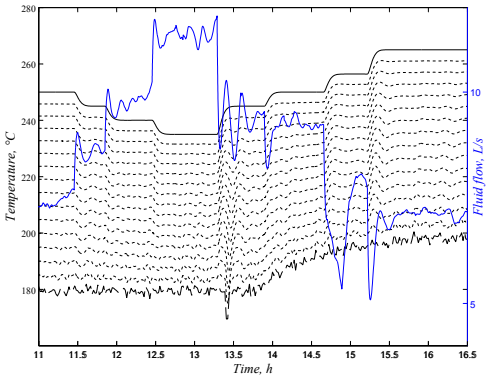

Figure 11: Inlet, outlet and segments temperatures of fluid in 2-D for the tube with the flow.

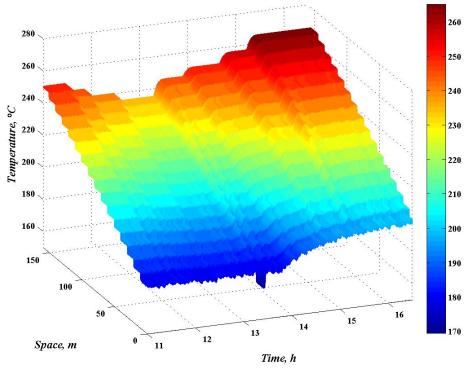

Figure 12: Internal dynamics showing the temperature distribution in 3D.

4.2 Robustness tests

In this part, some robustness tests are given to show the difference between the two controllers. This robustness will be supposed against both the modelling errors and the system parameters variations over time, such as fluid density and thermal capacity.

The first test will correspond to the increase in fluid density by 15 % ($\rho_{f_1} = 1.15\ \rho_{f_0}$). see Fig. 13, and the second will correspond to the decrease in fluid thermal capacity by 15 % ($C_{f_1} = 0.85\ C_{f_0}$), see Fig. 14.

As seen in the two figures, the CDM controller is more robust against the parameters variations.

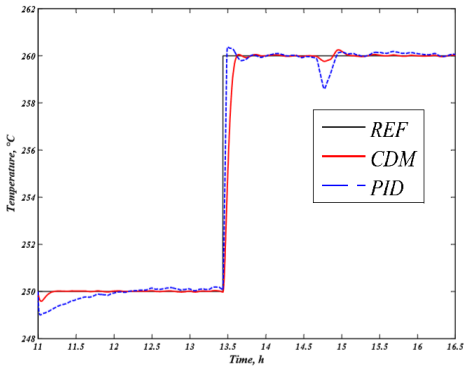

Figure 13: Responses in case of fluid density increase.

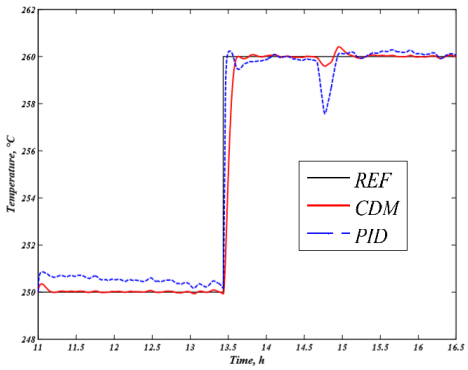

Figure 14: Responses in case of thermal capacity decrease.

5 Conclusion

In this work, a control system for the cylindrical-parabolic collector of a solar plant is designed employing the coefficient diagram method (CDM), which is an algebraic method. The cylindrical-parabolic solar collector is considered as an uncertain non-linear system, represented by two partial differential equations (PDEs), that usually complicates the control.

The performance and robustness of the CDM-controller has been tested with digital simulations using Matlab functions and Simulink programs. The CDM results have been compared with those of the PID-controller. It is shown by the comparative design examples in Section 4, that the controlled system using the CDM exhibits better performance than the PID-control with the external disturbances. The designed controller is simple, easy, robust against parameter variations, capable of decreasing the steady state error to zero and reducing the settling time (even with a large rise time), while supervising an admissible pump control signal applied to the actual plant, which may give a significant life to the pump.

Therefore, the CDM is flexible and can be used perfectly for the precise control in different conditions, replacing the traditional PID and LQG controllers and others (it is important to note that the PID controller may assume the control object as seen in different works, also the LQG controller has the same form as the CDM one, but the CDM controller synthesis is easier and have better performance and more robustness).

We also remind that it is still necessary to make a system of CDM controllers combined with fuzzy logic to ensure the control with all parameter variations such as solar radiation, inlet temperature and reference temperature, as done in [25]

References

[1] S. Elmetennani and T.M. Laleg-Kirati. Bilinear reduced order approximate model of parabolic distributed solar collectors. *Solar Energy* **131** (2016) 71–80.

[2] E. F. Camacho, F. R. Rubio, and F. M. Hughes. Self-tuning control of a solar power plant with a distributes collector field. *IEEE Control Systems* (1992) 72–78.

[3] E. F. Camacho and E. Berenguel. Robust adaptive model predictive control of a solar plant with bounded uncertainties. *International Journal of Adaptive Control and Signal processing* **11**(4) (1997) 311–325.

[4] E.F. Camacho, F.R. Rubio, M. Berenguel, and L. Valenzuela. A survey on control schemes for distributed solar collector fields. part ii : Advanced control approaches. *Solar Energy* **81** (2007) 1252–1272.

[5] E.F. Camacho, F.R. Rubio, M. Berenguel, and L. Valenzuela. A survey on control schemes for distributed solar collector fields. part i : Modeling and basic control approaches. *Solar Energy* **81** (2007) 1240–1251.

[6] C. Cirre, L. Valenzuela, M. Berenguel, and E. F. Camacho. Feedback linearization control for a distributed solar collector field. *IFAC Proceedings Volumes* **38**(1) (2005) 356–361.

[7] R. N. Silva, L. M. Rato, L. M. Barao, and J. M. Lemos. A physical model based approach to distributed collector solar field control. In: *Proceedings of the American Control Conference, Anchorage, AK* (2002) 3817–3822.

[8] F. R. Rubio, M. Berenguel, and E. F. Camacho. Fuzzy logic control of a solar power plant. *IEEE Transactions on Fuzzy Systems* **3**(4) (1995) 459–468.

[9] D. Limon, I. Alvarado, T. Alamo, M. Ruiz, and E. F. Camacho. Robust control of the distributed solar collector field acurex using mpc for tracking. *Proceedings of the 17th World Congress The International Federation of Automatic Control* (2008) 958–963.

[10] E. F. Camacho and A. J. Gallego. Estimation of effective solar irradiation using an unscented kalman filter in a parabolic-trough field. *Solar Energy* **86** (2012) 3512–3518.

[11] S. F. AVSAR and M. T. Soylemez. Optimizing cdm controllers under control signal constraints. In: *International Symposium on Innovations in Intelligent Systems and Applications, IEEE*, (2012).

[12] K. Kalpana and B. Meenakshipriya. Design of coefficient diagram method (cdm) based pid controller for double integrating unstable system. In: *2nd International Conference on Electrical Energy Systems (ICEES), IEEE*, (2014).

[13] S. Manabe. Coefficient diagram method as applied to the attitude control of controlled-bias-momentum satellite. In: *13th IFAC Symposium on Automatic Control in Aerospac, Palo Alto, California, USA*, (1994) 322–327.

[14] M. KoksalL and S. E. Hamamci. A program for the design of linear time invariant control systems : Cdmcad. *Computer Application and Engeneering Education* **12** (2004) 165–174.

[15] O. Ocal, M.T Soylemez, and A. Bir. Robust controller tuning based on coefficient diagram method. In: *Proceedings of International Conference on Control, Manchester, UK*, 2008.

[16] S.E. Hamamci and M. Koksal. Robust control of a dc motor by coefficient diagram method. In: *Proceedings of the 9th Mediterranean Conference on Control and Automation, Dubrownik, Chorwacja*, 2001.

[17] E. F. Camacho, M. Berenguel, F. R. Rubio, and D. Martinez. *Advanced Control of Solar Thermal, Control of Solar Energy Systems. Springer, London Dordrecht Heidelberg, New York*, 2012.

[18] A.J. Gallego and E.F. Camacho. Adaptative state-space model predictive control of a parabolic-trough field. *Control Engineering Practice* **20** (2012) 904–911.

[19] S. Manabe. Brief tutorial and survey of coefficient diagram method. In: *The 4th Asian Control Conference, Singapore* (2002) 1161–1166.

[20] R. Ali, T. H. Mohamed, Y. S. Qudaih, and Y. Mitani. A new load frequency control approach in an isolated small power systems using coefficient diagram method. *Electrical Power and Energy Systems* **56** (2014) 110–116.

[21] M. Z. Bernard, T. H. Mohamed, Y. S. Qudaih, and Y. Mitani. Decentralized load frequency control in an interconnected power system using coefficient diagram method. *Electrical Power and Energy Systems* **63** (2014) 165–172.

[22] H. Kim. The study of control design method. *IEEE, Information Technology, KORUS* (2004) 55–58.

[23] P.V. Gopi Krishna Rao, M. V. Subramanyam, and K. Satyaprasad. Study on pid controller design and performance based on tuning techniques. In: *International Conference on Control, Instrumentation, Communication and Computational Technologies (ICCICCT)* (2014) 1411–1417.

[24] C. A. Mosbah, M. Tadjine, M. Chakir, and M. S. Boucherit. On the control of parabolic solar collector : The zipper approach. *International Joural of Renewable Energy Research* **6**(3) (2016) 1100–1108.

[25] A. L. Cardoso, J. Henriques, and A. Douardo. Fuzzy supervisor and feedforward control of a solar power plant using accessible disturbances. In: *European Control Conference (ECC), IEEE*, 1999.

[26] P. Garasi, Y. Qudaih, R. Ali, M. Watanabe, and Y. Mitani. Coefficient diagram method based load frequency control for a modern power system. *Journal Of Electronic Science And Technology* **12**(3) (2014) 270–276.

[27] A.A. Boichuk and V.F. Zhuravlev. Solvability criterion for integro-differential equations with degenerate kernel in banach spaces. *Nonlinear Dynamics and Systems Theory* **18**(4) (2018) 331–341.

[28] N. Fallo and R.J. Moitsheki. Approximate analytical solutions for transient heat transfer in two-dimensional straight fins. *Nonlinear Dynamics and Systems Theory* **19** (1-SI) (2019) 133–140.

[29] E. F. Camacho and A. J. Gallego. Optimal operation in solar trough plants: A case study. *Solar Energy* **95** (2013) 106–117.